In vitro Cytotoxic Evaluation of Metallic and Magnetic DNA-Templated Nanostructures

Hamsa Jaganathan[†] and Albena Ivanisevic[*,†,‡]

Weldon School of Biomedical Engineering and Department of Chemistry, Purdue University, West Lafayette, Indiana 47906

ABSTRACT We evaluate the potential in vitro cytotoxicity that may arise from metallic and magnetic DNA-templated nanostructures. By using a fluorescence-based assay, the viability of cells was examined after treatment with DNA-templated nanostructures. Inductively coupled plasma mass spectrometry (ICP-MS) was used to quantify the amount of nanoparticles internalized by the cells. Cell uptake of DNA-templated nanostructures was enhanced after encapsulating the nanostructure with layers of polyelectrolytes (PSS and PAH) and targeting ligands. Transmission electron microscope (TEM) images provided evidence that the nanostructures were localized in vesicles in the cytoplasm of the cells. The results from this study suggest that gold, iron oxide, and cobalt iron oxide DNA-templated nanostructures do not induce in vitro toxicity.

KEYWORDS: DNA template • gold nanoparticles • iron oxide nanoparticles • cobalt iron oxide nanoparticles • in vitro • cytotoxicity

INTRODUCTION

Increasing the number of nanotoxicology studies is becoming of critical importance because of a great interest in utilizing nanomaterials as medical diagnostic and therapeutic agents. Many research groups have been documenting nanotoxicology, or the study of toxic effects of nanosized structures (1−8). Acquiring the knowledge of possible toxic responses from nanomaterials is an important step toward the development of in vivo applications, such as implantable biomedical sensors and imaging agents (9). Different materials, including metals and magnets, are currently being explored as potential imaging agents for medical diagnostics. Metal materials, such as gold, exhibit unique optical properties that can be used for biomedical imaging applications. Gold nanoparticles (NPs) have been successfully utilized as imaging agents using reflectance microscopes for cancer cell biomarker imaging (10, 11). They also been used as contrast agents in X-ray computed tomography (12) and in optoacoustic tomography for deep tumor imaging (13). Magnetic materials, such as iron oxide (14), exhibit superparamagnetic properties that make them good candidates for new types of contrast agents for imaging of tumor tissues in magnetic resonance imaging (MRI) (15). As researchers continue to develop various structural and material designs and demonstrate their utility as nanosized imaging agents, there are concerns with respect to health and environmental safety, as well as potential side effects arising from the physicochemical properties of these materials.

Herein, cellular toxicity, uptake, and responses due to DNA-templated nanostructures are evaluated. More specifically, we focus on understanding effects from gold, iron oxide, and cobalt iron oxide NP constructs under in vitro conditions. In recent years, our group has studied the properties of self-assembled, DNA-templated nanostructures. As cationic ligand coated NPs (~5 nm) electrostatically interact with the anionic charged backbone of DNA strands, the NPs align along the DNA strands, forming one-dimensional, nanoparticle chains (16). Previously, gold nanoparticles aligned along DNA strands have exhibited to be an ordered, controlled structure (17). In addition, cobalt iron oxide nanoparticles templated on DNA displayed high saturation magnetization (18). Furthermore, iron oxide nanoparticles arranged on single-stranded DNA demonstrated high magnetic relaxation rates (19). These studies show evidence that the physical properties of NPs were enhanced due to the one-dimensional arrangement onto DNA strands. Although toxic effects from one-dimensional nanostructures, such as carbon nanotubes (20−22), have been studied extensively, more studies are needed to determine the toxic effects from one-dimensional nanostructures scaffolded by biomolecules, such as linear peptides and DNA. As many research groups are interested in the development of DNA-templated nanostructures (17, 23−31), there is a need to assess the potential adverse effects that may arise when using DNA-templated nanostructures, as they have various applications in medicine and biology.

In this paper, in vitro effects due to metallic and magnetic DNA-templated nanostructures were studied as an initial step toward potential in vivo applications in medical imaging. Cellular toxicity arising from DNA-templated nanostructures was assessed by a fluorescence-based assay. DNA-templated nanostructures were them encapsulated by multiple layers of oppositely charged polyelectrolytes using

* Corresponding author. E-mail: albena@purdue.edu.
Received for review January 19, 2010 and accepted April 19, 2010
† Weldon School of Biomedical Engineering, Purdue University.
‡ Department of Chemistry, Purdue University.
DOI: 10.1021/am1000568

the layer-by-layer (LBL) method. Subsequently, the toxicity effects that might arise from the presence of polyelectrolytes were studied. Furthermore, targeting peptides were electrostatically attached to the outer surface of LBL-encapsulated, DNA-templated nanostructures to examine changes in cellular uptake. In addition, transmission electron microscope (TEM) images were collected to investigate changes in morphology of the nanostructure after cellular internalization. The results from this study suggest that cytotoxicity is decreased and cell uptake is increased when DNA-templated nanostructures are encapsulated with polyelectrolytes, and terminated with targeting peptides.

EXPERIMENTAL METHODS

Materials. Poly-L-lysine-coated gold NPs (~5 nm) were purchased from Ted Pella, Inc. (Redding, CA), and pyrrolidinone-coated iron oxide and cobalt iron oxide NPs were synthesized in our lab, following a literature protocol from Li et al. (32). Characterization of the nanoparticles can be found in Jaganathan et al. (16). Unmethylated lambda phage DNA and 10× MULTI-CORE buffer were purchased from Promega. Both polyelectrolytes, poly(styrene sulfonate) (PSS, MW ~70 000) and poly(allylamine hydrochloride) (PAH, MW ~70 000) were purchased from Sigma-Aldrich. The peptide with sequence of KKKKKKRGD (MW 1116.4, purity >95%) was synthesized and purified by Biosynthesis Inc. (Lewisville, TX).

Nanoparticle Washing. Gold, iron oxide, and cobalt iron oxide NPs were washed in water by centrifuging for 10 min at 13 000 rpm. This washing process was repeated 3−5 times before cells were treated with washed NPs. Washed NPs (30 μL) added to fresh medium (70 μL) were used to treat cells.

Fabrication of LBL-Encapsulated, DNA-Templated Nanostructures. DNA-templated nanostructures were formed by vortexing a solution of unmethylated lambda phage DNA (536 μg/mL) and nanoparticles (1 mg/mL) in 1X MULTI-CORE buffer for 1 h at room temperature. For a nanostructure with mass ratio of 1:1 DNA:NP, equal volumes of DNA and NPs are added to the solution. Other nanostructures with mass ratios of 1:5 and 1:25 DNA:NP are formed similarly with the volume of nanoparticle being 5 and 25 times the volume of DNA added to the solution, respectively.

For the LBL encapsulation, PSS and PAH polyelectrolytes were used only for the DNA-templated nanostructure with 1:1 DNA:NP mass ratio. First, PSS (1 mg/mL) was added to the DNA-templated nanostructure solution and vortexed for 15 min at room temperature. PAH (1 mg/mL) was then added to the solution and vortexed for another 15 min at room temperature. The layering of PSS and PAH was repeated up to seven times. As the eighth layer, RGD-terminated poly-L-lysine peptide chains (1 μg/mL) were added and vortexed for 15 min. This washless process for layer-by-layer encapsulation was first reported by Bantchev et al. (33).

Dynamic Light-Scattering Measurements. Sizes of the various constructs of nanostructures were determined using a Zetasizer Nano-ZS90 (Malvern Instruments, Worcestershire, U.K.). Concentration of DNA in DNA-templated nanostructures before and after LBL encapsulation was approximately 13 μg/mL for all size measurements. Nanostructures were diluted in MULTI-CORE buffer before testing and the readings were measured three times at room temperature.

Culturing HT-29 Cell Line. Human colon cancer cell line (HT-29 cells, purchased in American Type Culture Collection (ATCC)) were cultured in McCoy's 5A medium (ATCC, Manassas, VA) in BD Falcon T-25 cell culture flasks. McCoy's 5A medium was supplemented with 10% fetal bovine serum (ATCC). The cell culture was incubated and maintained in 37 °C in an atmosphere of 5% CO_2 and 95% relative humidity. Cells were 50% confluent by 2 days. Fresh medium was changed twice a week and cells were passed every week.

Cell Viability Experiments. Confluent HT-29 cells were washed with sterilized PBS (pH 7.4) and removed from the flask by trysin/EDTA (ATCC). After spinning the cells in a centrifuge (125g, 7 min), the pelletted cells were resuspended with fresh medium, and 10^4 cells (100 μL) were dispensed into 96-well flat bottom black plates for cell viability studies. Cells were seeded in triplicates for each treatment and allowed to attach to the surface for 24 h. Solutions containing the nanoconstructs (30 μL) were diluted in fresh media (70 μL) and added to the wells to treat the cells for the desired time durations (15 min to 6 days). The CellTiter-Blue Assay from Promega was used to assess cell viability. This assay provides a fluorometric method for quantifying the number of viable cells. The dye, resazurin, reduces to resorufin in viable cells. Resorufin is highly fluorescent, and nonviable cells will not generate the fluorescent signal. The resazurin dye (10 μL) was added to each well after the specified treatment time and incubated for 1 h in 37 °C in an atmosphere of 5% CO_2. The fluorescent intensity ($560_{Ex}\backslash 590_{Em}$), which is linearly proportional to the number of viable cells, was measured using the SpectraMax M5 Spectrophotometer (Molecular Devices, Sunnyvale, CA). Fluorescence emitted from artifacts, such as the medium alone, was measured and subtracted from the fluorescence emitted from the treated cells.

Preparation of Cells for Transmission Electron Microscopy. Cells were seeded in tissue culture plates and allowed to grow for three days. Solutions containing the nanoconstructs (1 mL) were prepared with fresh medium (2 mL) and incubated with the cells for 1 and 2 days before cell fixation. The microwave method was used to fix the cells on TEM grids. Glutaraldehyde (2%) in cacodylate buffer (0.1 M, pH 7.4) was allowed to react with the cells and was washed twice with cacodylate buffer and once with water. Osmium (1% in 1.5% $K_3Fe(CN)_6$) was then reduced and washed with water twice. Using a scraper, cells were removed from the dish and transferred into a centrifuge tube to be spun down. Agrose gel was added to the pelletted cells and cells were dispersed gently. After spinning down the cell/agrose gel pellet, the gel was cooled and removed with 10% ethanol. Samples were then diced and dehydrated by ethanol and propylene oxide. Embedding of the sample occurred through polymerization for 48 h at 60 °C. TEM grids were stained with 2% UA in 70% methanol for 5 min and lead citrate for 3 min. Samples were viewed on the FEI/Philips CM-10 BioTwin transmission electron microscope (FEI Company, Hillsboro, OR) using an accelerating voltage of 80 kV.

Quantifying Nanostructure Uptake in Cells by Inductively Coupled Plasma Mass Spectrometry. Cells (1×10^4 cells/100 μL) were seeded in triplicates in 96-well plates for each treatment and allowed to attach to the surface for 24 h. Solutions containing the nanoconstructs (30 μL) were diluted in fresh media (70 μL) and added to the wells to treat the cells for two days. After treatment, the medium from each sample in the well plate was collected and sonicated for 24 h. In addition, an initial solution of the nanostructures in medium was prepared and sonicated for 24 h. All sonicated samples with magnetic nanostructures were then digested in 70% HNO_3 (ARISTAR ULTRA, VWR) for 24 h. The samples were then diluted in 2% HNO_3 for ICP-MS measurements. For nanostructures with gold nanoparticles, samples were digested in aqua regia (3:1 HCl:HNO_3) for 24 h. Gold samples were then diluted in 2% aqua regia and sonicated for another 1 h before ICP-MS measurements. Elemental analysis for iron, cobalt, and gold was carried out using ThermoFinnigan ELEMENT2 inductively coupled argon plasma mass spectrometer system. Raw intensities of metal compositions were subtracted from intensities of a blank sample, which consisted of only the solvent (i.e., 2% aqua regia and 2% HNO_3). T ensure that any formation of metal complexes

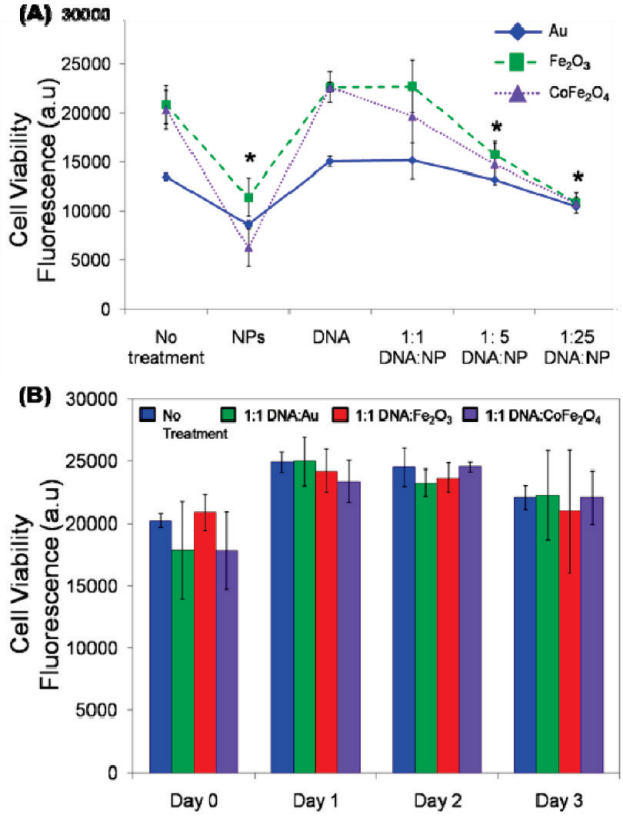

FIGURE 1. (A) Fluorescence measurements of viable cells after 24 h treatment of DNA-templated nanostructures at various mass ratios for gold, iron oxide, and cobalt iron oxide materials. (*) indicates significant difference compared to control (no treatment) at $p < 0.05$, $n = 9$. (B) Time study of viable cells after treatment of 1:1 DNA:NP nanostructures for gold, iron oxide, and cobalt iron oxide materials, no significant difference compared to control cells ($n = 9$).

with proteins did not skew the results, a known metal concentration of the nanoparticles in media was measured and compared to an equal metal concentration of the nanoparticles in water (shown in the Supporting Information, Table S1).

Statistical Analysis. Test for significance between groups were performed using one-way analysis of variance in STATA 10.0 (StataCorp LP, College Station, TX).

RESULTS AND DISCUSSION

Study of Cytotoxicity from DNA-Templated Nanostructures. In the reported proof-of-concept studies, the HT-29 cell line (human colon cancer cells) was used to study cytotoxic effects from DNA-templated nanostructures. The rezasurin assay, also called Alamar blue, measures viability by quantifying cell proliferation as a result of metabolic activity. This assay is advantageous because it provides a more feasible sample preparation than the popular MTT assay (9). Viability was measured after treating cells with gold, iron oxide, and cobalt iron oxide NPs for 24 h. Figure 1A displays that cell viability was significantly lower after treating with NPs compared to control cells, which were not subjected to any treatment and only incubated with fresh medium. Alkilany et al. reported that the starting materials and other molecules in the NPs buffer may be the primary factor for cytotoxicity. Whereas iron oxide and cobalt iron oxide NPs were synthesized in our lab and suspended in water, gold NPs were purchased from Ted Pella, Inc. The buffer for the gold NPs contained Tris(trishydroxymethyl-aminomethane), sodium azide, NaCl, BSA, and glycerol at a pH of 8.2. To test whether the NPs buffer or the NPs themselves caused cytotoxicity, we washed NPs three times and resuspended them in water. After treating the cells with washed NPs for 24 h, results, shown in the Supporting Information (Figure S1), suggest that washed gold NPs were not toxic to the cells, and cytotoxicity was induced from the NPs buffer. Magnetic NPs were toxic to cells, regardless of how many times they were washed.

Three different DNA-templated nanostructures were constructed by varying the mass ratio of DNA to NPs for gold, iron oxide, and cobalt iron oxide. All three types of NPs were washed before DNA-templated nanostructures were constructed. As the concentration of NPs increased in DNA-templated nanostructures, the viability of the cells decreased (Figure 1A). To confirm the results from the alamar blue assay, we used the trypan blue exclusion method (see the Supporting Information, Figure S2). Cells incubated with 1:1 DNA:NP for gold, iron oxide, and cobalt iron oxide, however, had no change in cell viability compared to cells with no treatment and cells treated with double-stranded, lambda phage DNA alone. When compared to the control cells, cells treated with nanostructures, constructed at a mass ratio of 1:1 DNA:NP for all three materials, demonstrated no cytotoxic effects for 3 days of treatment (Figure 1B). The time point, day 0, is counted as the measurement exactly after nanostructures/medium solution was added to the cells. The observable increase in fluorescence between day 0 and day 1 may be attributed to the growing number of viable cells in the Petri dish because of fresh media. The fluorescence after day 1 exhibits no change, demonstrating that the cells remained viable.

To gain a further understanding of the stability of DNA-templated nanostructures in a cellular environment, TEM images were collected after treating HT-29 cells with gold, iron oxide, and cobalt iron oxide nanoconstructs. The Supporting Information contains TEM images of HT-29 cells without treatment as control (Figure S3) and TEM images of HT-29 cells that were treated with cationic ligand coated gold, iron oxide, and cobalt iron oxide NPs (Figure S4). Control cells were healthy, clearly displaying images of identifiable nucleus and normal-sized mitochondria. In addition, there were no signs of vesicle formation in the control cells. Cells treated with NPs, however, displayed swelled mitochondria, representing unhealthy cells. Nanoparticles were found in clusters in vesicles and did not exhibit monodispersity. For a single cell, multiple numbers of vesicles were observed that entrapped the NPs. In addition, in the two day treatment, NPs did not enter the nucleus of the cells. It has been reported by others that positively charged NPs can be internalized by cells, regardless of size and charge distribution (34). We confirmed this nonspecific behavior of cell uptake for cationic NPs for all three materials. These types of results demonstrate that for bioimaging applications where targeting and localization in specific

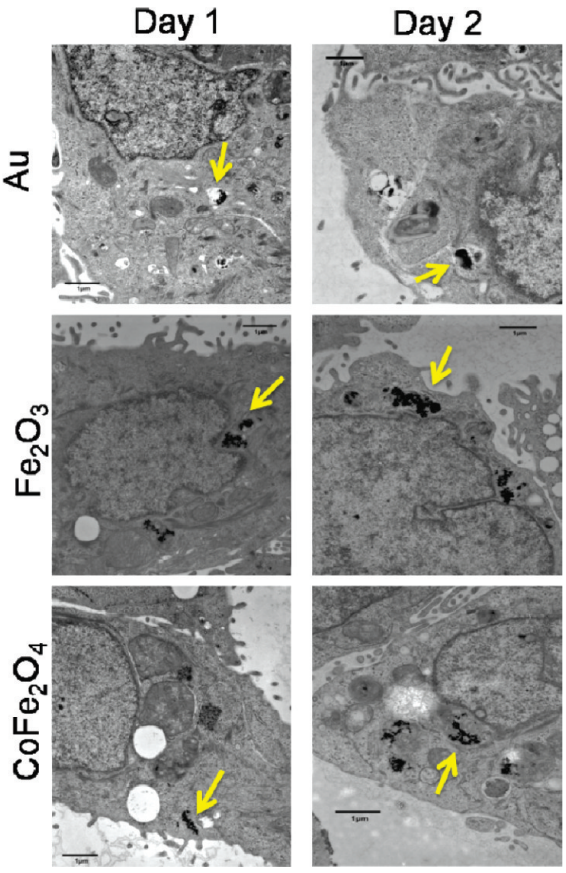

FIGURE 2. TEM images of HT-29 cells incubated with 1:1 DNA:NP nanostructures for gold, iron oxide, and cobalt iron oxide materials for 24 and 48 h. The yellow arrow on each image points to an example of the location of nanostructure after uptake in cells. The scale bar is 1 μm.

tissues is desired, NPs that are stabilized only by simple ligands may not be a suitable choice.

We have previously reported that the mass ratio of 1:1 DNA:NP is a stable, one-dimensional structure and is primarily governed by the electrostatic interactions between cationic ligand coated nanoparticles and the anionic phosphate backbone of DNA (16). Despite the charge distributions presented on the surface of the nanostructures, TEM images display that HT-29 cells were able to internalize metallic and magnetic DNA-templated nanostructures within 24 h of treatment (Figure 2). Cells were observed to be healthy and the mitochondria in the single cells were not swelled. NPs and DNA-templated nanostructures for all three materials were found in multiple vesicles in the cytoplasm of the cells. NPs were found in large aggregated groups in vesicles, as similar to DNA-templated nanostructures for all three materials. It is, however, observed that the size of the vesicles were greater than vesicles that contained NPs alone. The morphology of DNA-templated nanostructures did not attain a linear NP chain in the cell; rather, the nanostructures were in a tangled, clumped arrangement. Furthermore, it was observed that images after two days of treatment displayed larger-sized aggregations of nanostructures in the vesicles when compared to one day of treatment, meaning higher concentrations of DNA-templated nanostructures were internalized. Similar to NPs, DNA-templated nanostructures did not enter the nucleus of the cells. Previously, it was reported that the cationic NPs lose their electrostatic affinity to the DNA backbone and NPs disassociate from the DNA strands in a cellular environment (35). TEM images show that the internalization of the DNA-templated nanostructures for gold, iron oxide, and cobalt iron oxide in the cell is organized in vesicles after 1 and 2 days of treatment. However, one cannot observe whether disassociation of DNA from the NPs occurred using these images. There is a possibility that other cell internalization mechanisms may have governed the aggregation of the nanostructures, such as assistance from cellular proteins.

Study of Cytotoxicty after LBL Encapsulation. Nanostructures that are intended for in vivo applications need surface coatings to improve biocompatibility, reduce any immunological responses, and possibly aid in the controlled delivery of drugs and other materials. The layer-by-layer encapsulation is advantageous because it can coat nanostructures with nanometer thickness that supports various sizes and shapes (36). For DNA-templated nanostructures with a 1:1 DNA:NP mass ratio, negatively charged PSS and cationically charged PAH were alternatively layered on the nanostructures, starting with PSS as layer 1. The particle size measurements in DNA buffer is shown in Table 1. Sizes of the nanoparticle for gold, iron oxide, and cobalt iron oxide were measured higher than the sizes reported from AFM measurements (16). The increase in size is due to the effects from positively charged surface ligands attached to the nanoparticles. DNA-templated nanostructures were measured in buffer solution before and after they were encapsulated with polyelectrolytes. There was a significant increase in particle size after DNA-templated nanostructures were coated with polyelectrolytes (8 layers). The measurements confirm that DNA-templated nanostructures were encapsulated by the LBL method. The polydispersity index (PDI) provides a quantitative indication of the homogeneity of the nanoparticle size distribution. PDI values closer to 1 indicate more poly dispersed nanoparticle sizes. The PDI values measured for the nanostructures and DNA were all below 0.4, suggesting a relatively monodispersed size distribution.

After each stage of the layering process onto the DNA-templated nanostructures, the viability of cells was measured following a 24 h treatment. The addition of each layer (PSS and PAH) did not show any significant evidence of cytotoxicity for gold, iron oxide, and cobalt iron oxide nanostructures (Figure 3A). Although PAH alone was cytotoxic (see Figure S5 in the Supporting Information), nanostructures coated with PAH (layer 2, 4, and 6) were not cytotoxic. Alkilany et al. reported that the surface charge exhibited on nanostructures from the LBL method does not induce toxicity in cells (37). In addition, by assessing the viability at each stage of the layering process on the nanostructure, we can obtain initial evidence about cytotoxicity from potential surface degradation of the nanostructures that may occur in a cellular environment. The results suggest that the long-term effect of surface layer degradation of nanostructures will not affect the overall viability of the cells.

Table 1. Average Particle Sizes of DNA-Templated Nanostructures Measured at Room Temperature

				before LBL encapsulation		after LBL encapsulation	
	particle size (nm)[a]	polydispersity index (PDI)		particle size (nm)[a]	PDI	particle size (nm)[a]	PDI
DNA	96.7 ± 32.2	0.3					
Au NPs	169.8 ± 1.6	0.1	DNA:Au	118.2 ± 21.7	0.4	206.1 ± 6.6	0.3
Fe2O3 NPs	229.2 ± 25.1	0.3	DNA:Fe_2O_3	1566.0 ± 99.1	0.4	2797.5 ± 4.9	0.3
CoFe2O4 NPs	237.6 ± 23.8	0.3	DNA:$CoFe_2O_4$	622.6 ± 44.9	0.4	2358.5 ± 47.2	0.3

[a] Data represent average ± standard deviation ($n = 3$).

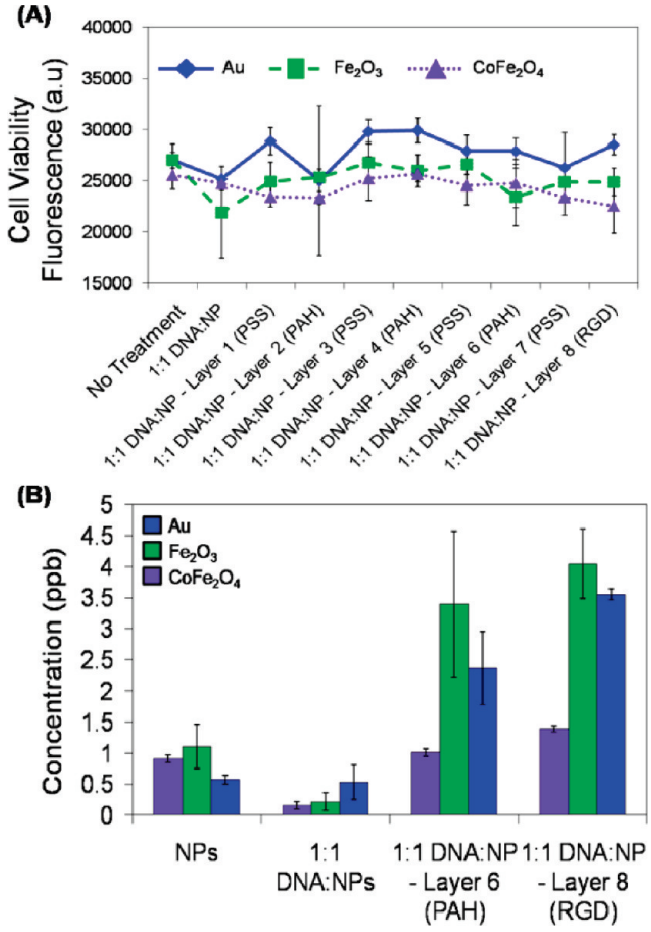

FIGURE 3. (A) Fluorescence measurement of viable cells after 24 h treatment after each polyelectrolyte layer was added onto DNA-templated nanostructures for gold, iron oxide, and cobalt iron oxide materials ($n = 9$). (B) HT-29 cell uptake after 2 days incubation of DNA:NP nanostructures for gold, iron oxide, and cobalt iron oxide nanostructures ($n = 3$).

As outer surface ligands (layer 8) of the nanostructure, RGD-terminated, poly-L-lysine peptide chains were electrostatically attached to the anionic polyelectrolyte layer, PSS (layer 7). RGD peptides strongly bind to integrin cell surface receptors. Cancer cells, such as the HT-29 cell line, are known to overexpress integrin receptors (38). Attaching RGD peptides to the outer surface of the nanostructures aids in effective tumor targeting, which is an essential function for in vivo imaging agents. Therefore, preliminary targeting efficacy was studied in vitro.

Inductively coupled plasma mass spectrometry (ICP-MS) was used to quantify the amount of nanostructures internalized by HT-29 cells. The initial elemental concentration for gold nanostructures in cell media was measured before treating cells. After a 2-day treatment with gold nanostructures, the medium from the treated cells was collected and analyzed by ICP-MS for the elemental concentration of gold. The difference between the initial gold concentration and the gold concentration after a 2-day treatment quantifies the amount of gold nanostructures that were internalized by the cells. This method of quantification was performed for iron oxide and cobalt iron oxide nanostructures as well. Figure 3B compares the cell uptake for four different constructs, including (1) NPs alone, (2) DNA-templated nanostructures at 1:1 DNA:NP mass ratio, (3) DNA-templated nanostructures coated with six polyelectrolyte layers, and (4) RGD-terminated, LBL-encapsulated nanostructures. A detailed significance test between and among groups is provided in the Supporting Information (Figure S6). NPs and the 1:1 DNA:NP construct demonstrated low cell uptake. It is speculated that nanoparticles and DNA-templated nanostructures are internalized by the mediation of nonspecific serum protein adsorption. Chithrani et al. concluded that cells were able to internalize more NPs than nanorods (elongated nanostructures) due to the difference in shapes (39). In this study, ICP-MS results of cell internalization displayed no significant difference between NPs and DNA-templated nanostructures. While the nanostructure constructed with 1:1 DNA:NP mass ratio exhibits an elongated shape, the flexible nature of the nanostructure allowed for the uptake in cells by tangling and agglomeration of the DNA strands, which is evident in the TEM images. Cell uptake was improved by encapsulating the DNA-templated nanostructures with polyelectrolyte layers, as observed after terminating the surface with PAH as the sixth layer. An enhancement of cell uptake after LBL encapsulation was also observed with gold nanorods by Hauck et al. (40).

Furthermore, the electrostatic attachment of targeting peptides demonstrated a significant difference in cell uptake compared to NPs and DNA-templated nanostructures. This high uptake of RGD coated nanostructures in cancer cells is consistent with other studies on RGD-terminated NPs (41) and RGD-terminated microspheres (42). In addition, a recent study consisting of iron oxide nanoparticle chains, called nanoworms, demonstrated to target cells more efficiently than NPs because of its elongated shape (43). An elongated shape provides more surface area for a greater number of ligand attachments. In turn, this increases the binding interactions between the cell surface receptor and the targeting ligand, which can account for the significant increase in cell uptake of RGD-terminated nanostructures.

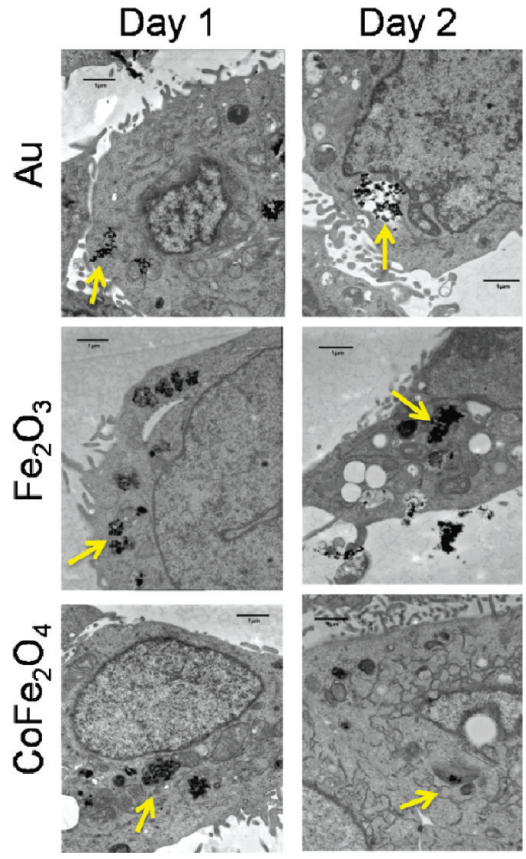

FIGURE 4. TEM images of HT-29 cells incubated with RGD-terminated, LBL-encapsulated 1:1 DNA:NP nanostructures for gold, iron oxide, and cobalt iron oxide materials for 24 and 48 h. Yellow arrows indicate an example of the location of nanostructure uptake in cells. The scale bar is 1 μm.

Although the ICP-MS method for quantifying the amount of nanostructure internalization was adequate, the calculation does not account for nanostructures that may have simply adsorbed on the surface of the cells and have leached out of cells within 2 days. Although nanostructures adsorbed on the cell surface could not have been observed in TEM images, HT-29 cells after 1 day and 2 days treatment with RGD-terminated DNA-templated nanostructures displayed that no significant leaching had occurred for all three materials (Figure 4). The morphological stability of RGD-terminated, DNA-templated nanostructures was also evaluated. As examined similarly with NPs alone and DNA-templated nanostructures, RGD-terminated, DNA-templated nanostructures were aggregated into multiple vesicles in the cytoplasm of a single cell. Single cells displayed no sign of nanostructures entering the nucleus. It was observed, as similar to cells treated with DNA-templated nanostructures, that the sizes of the vesicles in the cytoplasm were larger than cells treated with NPs alone.

The efficiency of exocytosis is equally important to understand. The study from Chithrani et al. has extensively researched the behavior of exocytosis for different sizes and shapes of nanostructures (39). We speculate that our nanostructures may exhibit the same behavior that was found in their study. Small-sized NPs were removed from the cell faster than large size NPs. In addition, the elongated nanostructures had a slow removal rate when compared to spherical-shaped NPs. More studies would be necessary to confirm the exocytosis mechanism of DNA-templated nanostructures.

To understand the full extent on the toxicity of RGD-terminated, LBL-encapsulated nanostructures, the viabilities of HT-29 cells were assessed after 6 days. Cells were healthy up to day 6. There was a significant decrease in fluorescencet intensity at day 6 of the cell treatment with RGD-terminated, LBL-encapsulated nanostructures compared to the previous days (Figure 5). Cells that were treated with medium only had also a decrease in fluorescent intensity at day 6 (data not shown). Because the observed decrease in cell viability at day 6 may be due to the space availability of cells in a 96-well plate, the same experiment was performed in T-25 flasks to ensure space for cell growth; this result is presented in the Supporting Information (Figure S7). After the cells were seeded, the cell media containing DNA-templated nanostructures was changed for the cells, while the control cells were changed with fresh cell media every alternative day. It was found that cells treated with nanostructures had a significant decrease in cell viability at day 6 when compared to cells with no treatment. This decrease in cell viability is due to the accumulation of the nanostructures in the cells.

When nanostructures are incubated in cell media, it is important to verify that the nanostructures do not alter their morphology from surface adsorption of proteins and ions contained in the cell media. Especially when using the LBL method to form the nanostructures, the charge distribution on the nanostructure can be affected from the contents in cell media. Studies have demonstrated that LBL constructed nanostructures are stable and functions under in vitro conditions (41, 44, 45). We measured the average particle size of nanostructures in cell media after 1 day and 5 days of incubation, shown in the Supporting Information (Figure S8). Although it is difficult to determine the types of changes in

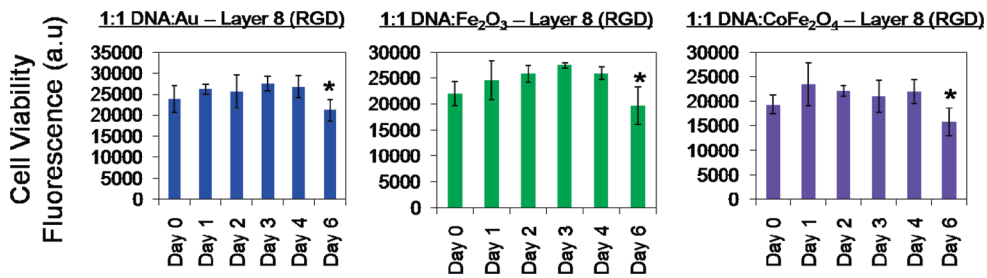

FIGURE 5. Time study for 6 days of viable cells after treatment of RGD-terminated, LBL-encapsulated 1:1 DNA:NP nanostructures for gold, iron oxide, and cobalt iron oxide materials. (*) indicates significance difference in viability compared to previous days at $p < 0.05$, $n = 9$.

morphology of the nanostructures in the cell media, the average particle size distribution in media decreased when compared to the average particle size distribution in buffer (listed in Table 1). We observed, however, that there was no significant difference in the average particle size between day 1 and day 5 of media incubation. Although protein complexes and adsorption may have occurred in the cell media solution, the results suggest that there were no changes in particle size distribution for long periods of time in media.

CONCLUSIONS

In summary, we assessed the toxicity effects from DNA-templated nanostructures in vitro. Although NPs alone appeared to be toxic to cells, gold, iron oxide, and cobalt iron oxide DNA-templated nanostructures did not affect cell viability. In addition, TEM images showed evidence that DNA-templated nanostructures were accumulated in vesicles in the cytoplasm. After the DNA-templated nanostructures were encapsulated with polyelectrolyte layers and terminated with targeting ligands, cell uptake was significantly enhanced. These types of results on the toxicity and localization of the nanostructures in the cytoplasm are critical before one proceeds with further studies that deal with in vivo intracellular and tissue imaging.

Acknowledgment. This work was supported by NSF under CMMI-0727927. We thank Debra M. Sherman and Chia-Ping Huang from Purdue University Life Science Microscopy Facility for their assistance with TEM instrument and Dr. Karl V. Wood, Dr. Rudiger Laufhutte, and Arlene Rothwell for their assistance with ICP-MS measurement and analysis. In addition, we thank Professor Yoon Yeo's lab for sharing their DLS instrument, and Professor Alyssa Panitch for sharing her UV—vis spectrophotometer.

Supporting Information Available: Plots of cell viability after nanoparticle washing and cell viability after treating with PAH, PSS, and RGD; TEM images of HT-29 cells with no treatment and TEM images of HT-29 cells treated with nanoparticles; significance tests on cell uptake, plots of cell viability, DLS experiments, and ICP-MS data (PDF). This material is available free of charge via the Internet at http://pubs.acs.org.

REFERENCES AND NOTES

(1) King-Heiden, T. C.; Wiecinski, P. N.; Mangham, A. N.; Metz, K. M.; Nesbit, D.; Pedersen, J. A.; Hamers, R. J.; Heideman, W.; Peterson, R. E. *Environ. Sci. Technol.* **2009**, *43* (5), 1605–1611.
(2) Metz, K. M.; Mangham, A. N.; Bierman, M. J.; Jin, S.; Hamers, R. J.; Pedersen, J. A. *Environ. Sci. Technol.* **2009**, *43* (5), 1598–1604.
(3) Wiecinski, P. N.; Metz, K. M.; Mangham, A. N.; Jacobson, K. H.; Hamers, R. J.; Pedersen, J. A. *Nanotoxicology* **2009**, *3* (3), 202–214.
(4) Balbus, J. M.; Maynard, A. D.; Colvin, V. L.; Castranova, V.; Daston, G. P.; Denison, R. A.; Dreher, K. L.; Goering, P. L.; Goldberg, A. M.; Kulinowski, K. M.; Monteiro-Riviere, N. A.; OberdÃ¶rster, G. n.; Omenn, G. S.; Pinkerton, K. E.; Ramos, K. S.; Rest, K. M.; Sass, J. B.; Silbergeld, E. K.; Wong, B. A. *Environ. Health Perspect.* **2007**, *115* (11), 1654–1659.
(5) Zhang, L. W.; Yu, W. W.; Colvin, V. L.; Monteiro-Riviere, N. A. *Toxicol. Appl. Pharmacol.* **2008**, *228* (2), 200–211.
(6) Ryman-Rasmussen, J. P.; Riviere, J. E.; Monteiro-Riviere, N. A. *Nano Lett.* **2007**, *7* (5), 1344–1348.
(7) Hardman, R. *Environ. Health Perspect.* **2006**, *114*, 165.
(8) Jin, Y.; Kannan, S.; Wu, M.; Zhao, J. X. *Chem. Res. Toxicol.* **2007**, *20* (8), 1126–1133.
(9) Marquis, B. J.; Love, S. A.; Braun, K. L.; Haynes, C. L. *Analyst* **2009**, *134* (3), 425–439.
(10) Sokolov, K.; Follen, M.; Aaron, J.; Pavlova, I.; Malpica, A.; Lotan, R.; Richards-Kortum, R. *Cancer Res.* **2003**, *63* (9), 1999–2004.
(11) Javier, D. J.; Nitin, N.; Levy, M.; Ellington, A.; Richards-Kortum, R. *Bioconjugate Chem.* **2008**, *19* (6), 1309–1312.
(12) Kim, D.; Park, S.; Lee, J. H.; Jeong, Y. Y.; Jon, S. *J. Am. Chem. Soc.* **2007**, *129* (24), 7661–7665.
(13) Copland, J. A.; Eghtedari, M.; Popov, V. L.; Kotov, N.; Mamedova, N.; Motamedi, M.; Oraevsky, A. A. *Mol. Imaging Biol.* **2004**, *6* (5), 341–349.
(14) Chouly, C.; Pouliquen, D.; Lucet, I.; Jeune, J. J.; Jallet, P. *J. Microencapsul.* **1996**, *13* (3), 245–255.
(15) Gupta, A. K.; Gupta, M. *Biomaterials* **2005**, *26* (18), 3995–4021.
(16) Jaganathan, H.; Kinsella, J. M.; Ivanisevic, A. *ChemPhysChem* **2008**, *9* (15), 2203–2206.
(17) Nakao, H.; Shiigi, H.; Yamamoto, Y.; Tokonami, S.; Nagaoka, T.; Sugiyama, S.; Ohtani, T. *Nano Lett.* **2003**, *3* (10), 1391–1394.
(18) Kinsella, J. M.; Ivanisevic, A. *J. Phys. Chem. C* **2008**, *112* (9), 3191–3193.
(19) Byrne, S. J.; Corr, S. A.; Gun'ko, Y. K.; Kelly, J. M.; Brougham, D. F.; Ghosh, S. *Chem Commun* **2004**, (22), 2560–2561.
(20) Shi Kam, N. W.; Jessop, T. C.; Wender, P. A.; Dai, H. *J. Am. Chem. Soc.* **2004**, *126* (22), 6850–6851.
(21) Warheit, D. B.; Laurence, B. R.; Reed, K. L.; Roach, D. H.; Reynolds, G. A. M.; Webb, T. R. *Toxicol. Sci.* **2004**, *77* (1), 117–125.
(22) Sayes, C. M.; Liang, F.; Hudson, J. L.; Mendez, J.; Guo, W.; Beach, J. M.; Moore, V. C.; Doyle, C. D.; West, J. L.; Billups, W. E.; Ausman, K. D.; Colvin, V. L. *Toxicol. Lett.* **2006**, *161* (2), 135–142.
(23) Nakao, H.; Hayashi, H.; Yoshino, T.; Sugiyama, S.; Otobe, K.; Ohtani, T. *Nano Lett.* **2002**, *2* (5), 475–479.
(24) Braun, E.; Eichen, Y.; Sivan, U.; Ben-Yoseph, G. *Nature* **1998**, *391*, 775–778.
(25) Alivisatos, P. A.; Johnsson, K. P.; Peng, X.; Wilson, T. E.; Loweth, C. J.; Bruchez, M. P. J.; Schultz, P. G. *Nature* **1996**, *382*, 609–611.
(26) Coffer, J. L.; Bigham, S. R.; Li, X.; Pinizzotto, R. F.; Rho, Y. G.; Pirtle, R. M.; Pirtle, I. L. *Appl. Phys. Lett.* **1996**, *69*, 3851–3853.
(27) Ford, W. E.; Harnack, O.; Yasuda, A.; Wessels, J. M. *Adv. Mater.* **2001**, *13* (23), 1793–1797.
(28) Gu, Q.; Cheng, C.; Haynie, D. T. *Nanotechnology* **2005**, *16*, 1358–1363.
(29) Gu, Q.; Suryanarayanan, S.; Dai, K.; Haynie, D. T. *Physica E* **2006**, *33*, 92–98.
(30) Monson, C. F.; Woolley, A. T. *Nano Lett.* **2003**, *3* (3), 359–363.
(31) Deng, Z.; Mao, C. *Nano Lett.* **2003**, *3* (11), 1545–1548.
(32) Li, Z.; Chen, H.; Bao, H.; Gao, M. *Chem. Mater.* **2004**, *16* (8), 1391–1393.
(33) Bantchev, G.; Lu, Z.; Lvov, Y. *J. Nanosci. Nanotechnol.* **2009**, *9*, 396–403.
(34) Verma, A.; Stellacci, F. *Small* **2010**, *6* (1), 12–21.
(35) Han, G.; Chari, N. S.; Verma, A.; Hong, R.; Martin, C. T.; Rotello, V. M. *Bioconjugate Chem.* **2005**, *16* (6), 1356–1359.
(36) Ai, H.; Jones, S.; Lvov, Y. *Cell Biochem. Biophys.* **2003**, *39* (1), 23–43.
(37) Alkilany, A. M.; Nagaria, P. K.; Hexel, C., R.; Shaw, T. J.; Murphy, C. J.; Wyatt, M. D. *Small* **2009**, *5*, 701–708.
(38) O'Brien, V.; Frisch, S. M.; Juliano, R. L. *Exp. Cell Res.* **1996**, *224* (1), 208–213.
(39) Chithrani, B. D.; Ghazani, A. A.; Chan, W. C. W. *Nano Lett.* **2006**, *6* (4), 662–668.
(40) Hauck, T. S.; Ghazani, A. A.; Chan, W. C. W. *Small* **2008**, *4* (1), 153–159.
(41) Kim, J. S.; Rieter, W. J.; Taylor, K. M. L.; An, H.; Lin, W.; Lin, W. *J. Am. Chem. Soc.* **2007**, *129* (29), 8962–8963.
(42) Toublan, F. J.-J.; Boppart, S.; Suslick, K. S. *J. Am. Chem. Soc.* **2006**, *128* (11), 3472–3473.
(43) Park, J.-H.; Maltzahn, G. v.; Zhang, L.; Schwartz, M. P.; Ruoslahti, E.; Bhatia, S. N.; Sailor, M. J. *Adv. Mater.* **2008**, *20* (9), 1630–1635.
(44) Cortez, C.; Tomaskovic-Crook, E.; Johnston, A. P. R.; Scott, A. M.; Nice, E. C.; Heath, J. K.; Caruso, F. *ACS Nano* **2007**, *1* (2), 93–102.
(45) Itoh, Y.; Matsusaki, M.; Kida, T.; Akashi, M. *Biomacromolecules* **2008**, *9* (8), 2202–2206.

AM1000568